NMDA receptor–dependent dephosphorylation of serine 387 in Argonaute 2 increases its degradation and affects dendritic spine density and maturation

Received for publication, November 28, 2017, and in revised form, April 26, 2018 Published, Papers in Press, May 7, 2018, DOI 10.1074/jbc.RA117.001007

Nicolas Paradis-Isler[1] **and Jannic Boehm**[2]

From the Département Neurosciences, Groupe de Recherche sur le Système Nerveux Central, Université de Montréal, Montréal, Québec H3T 1J4, Canada

Edited by Paul E. Fraser

Argonaute (AGO) proteins are essential components of the microRNA (miRNA) pathway. AGO proteins are loaded with miRNAs to target mRNAs and thereby regulate mRNA stability and protein translation. As such, AGO proteins are important actors in controlling local protein synthesis, for instance, at dendritic spines and synapses. Although miRNA-mediated regulation of dendritic mRNAs has become a focus of intense interest over the past years, the mechanisms regulating neuronal AGO proteins remain largely unknown. Here, using rat hippocampal neurons, we report that dendritic Ago2 is down-regulated by the proteasome upon NMDA receptor activation. We found that Ser-387 in Ago2 is dephosphorylated upon NMDA treatment and that this dephosphorylation precedes Ago2 degradation. Expressing Ser-387 phosphorylation–deficient or phosphomimetic Ago2 in neurons, we observed that this phosphorylation site is involved in modulating dendritic spine morphology and postsynaptic density protein 95 (PSD-95) expression in spines. Collectively, our results point toward a signaling pathway linking NMDA receptor–dependent Ago2 dephosphorylation and turnover to postsynaptic structural changes. They support a model in which NMDA receptor–mediated dephosphorylation of Ago2 and Ago2 turnover contributes to the de-repression of mRNAs involved in spine growth and maturation.

Neuronal homeostasis requires a tight regulation of turnover for proteins involved in cellular signaling and structural adaptation (1, 2). More particularly, activity-dependent local protein synthesis has been shown to be necessary for several forms of synaptic plasticity (3–5). Consequently, many messenger RNAs (mRNAs) are transported to dendrites and then locally translated into proteins (6–9).

In recent years, microRNAs (miRNAs)[3] have emerged as key factors in post-transcriptional regulation for a majority of mRNAs (10, 11). miRNAs are short noncoding RNAs (~20–24 nucleotides) that target their complementary sequences in specific mRNAs, thereby causing the inhibition of translation and/or a decrease in mRNA stability (12–15). The prominent role of miRNAs in neurons has been underlined by the discovery that miRNAs are significantly involved in regulating neuronal morphology and function (6, 16–19).

The regulation of mRNA translation by miRNAs occurs in the miRNA-induced silencing complex (miRISC), which enables miRNAs to target their mRNAs (12, 14, 20, 21). Several studies have shown that the association of miRISC with different scaffold or RNA-binding proteins underlies the translational regulation associated with synaptogenesis and synaptic plasticity (22–27).

At the core of miRISCs are Argonaute (AGO) proteins, which are loaded with miRNAs and enable miRNAs to bind their target mRNAs and induce subsequent translational repression (12, 14, 20, 21). Mammals express four to five different AGO proteins as follows: Ago1–4 and in mouse Ago5 (28, 29). Ago1 and Ago2 are the predominant forms of AGO proteins in the brain (30). Ago2 is the only mammalian AGO protein to possess endonuclease activity, which is induced by siRNAs and catalyzes cleavage and rapid degradation of targeted mRNAs (31, 32). Several different post-translational modifications of Ago2, like phosphorylation or ubiquitination, have been shown to alter Ago2 subcellular localization, protein stability, and its interaction with RNAs (20, 33). Despite the importance of Ago2 as a core component in miRNA-mediated control of dendritic mRNA translation, the regulation of Ago2 in response to neuronal activity remains largely unknown.

Here, we report that Ago2 is down-regulated in a proteasome-dependent manner upon NMDA-receptor (NMDA-R) activation in cultured hippocampal neurons. We find that prior to Ago2 degradation, NMDA treatment causes dephosphoryla-

This work was supported in part by an operating grant from the "Natural Sciences and Engineering Research Council of Canada" (NSERC) Discovery Grant 371858. The authors declare that they have no conflicts of interest with the contents of this article.
This article contains Figs. S1–S5.
[1] Supported by Natural Sciences and Engineering Research Council of Canada (NSERC) "Alexander Graham Bell" master student stipend and a Ph.D. stipend from the Quebec "Fonds de Recherche Nature et Technologies" (FQRNT).
[2] Supported by a salary award from the "Fonds de Recherche Santé Québec" (FRQS). To whom correspondence should be addressed: Dépt. of Neurosciences, Université de Montréal, 2960 Chemin de la Tour, Montréal, Québec H3T 1J4, Canada; Tel.: 514 343 6370; E-mail: jannic.boehm@umontreal.ca.

[3] The abbreviations used are: miRNA, microRNA; siRNA, short-interfering RNA; AGO protein, Argonaute protein; miRISC, miRNA-induced silencing complex; PTX, picrotoxin; eGFP, enhanced green fluorescent protein; tdTomato, tandem-dimer Tomato fluorescent protein; NMDA, *N*-methyl-D-aspartate; DIV, days *in vitro*; ANOVA, analysis of variance; NMDA-R, NMDA receptor; P-bodies, processing bodies; mAb, monoclonal antibody; PVDF, polyvinylidene difluoride; PDL, poly-D-lysine; PFA, paraformaldehyde; APV, 2-amino-5-phosphonopentanoic acid.

tion of Ago2 at serine 387. Finally, we demonstrate that expression of Ser-387 phosphorylation-deficient Ago2 increases dendritic spine density and promotes features associated with spine maturation.

Results

NMDA-R activity regulates proteasomal degradation of dendritic Ago2

To analyze the effect of synaptic activity on Ago2 protein localization and turnover in dendrites, we briefly incubated mature dissociated hippocampal neuronal cultures with NMDA. Immunocytochemistry analysis revealed a significantly lower amount of dendritic Ago2 in neurons treated with NMDA compared with untreated neurons (Fig. 1*A*). To exclude that NMDA-dependent neurotoxicity might account for our effects, we performed trypan blue staining 24 h after treatment with different NMDA concentrations for different durations. As shown in Fig. S1, the employed NMDA concentration did not induce neurotoxicity. Next, we asked whether a more general increase in synaptic activity would also cause a reduction in dendritic Ago2. We therefore treated neuronal cultures with the $GABA_A$ antagonist picrotoxin (PTX) to generally increase synaptic transmission in our neuronal cultures. Incubation with PTX induced a significant loss of Ago2 in dendrites (Fig. S2), which was blocked by co-incubation with the NMDA-R antagonist APV (AP5) thereby indicating again that NMDA-R stimulation is causing the loss of Ago2. Having observed that NMDA-R stimulation leads to a down-regulation of dendritic Ago2, we turned our attention toward the underlying mechanism. It has been shown in several non-neuronal cell types that Ago2 protein levels are regulated by proteasomal degradation (34–37). In addition, synaptic activity and NMDA-R activation, in particular, are known to up-regulate the proteasomal pathway in dendrites and spines (38–42). We therefore hypothesized that NMDA-R activation could trigger proteasomal degradation of Ago2 in neuronal dendrites. To test this hypothesis, we added the proteasome inhibitor lactacystin 1 h prior to NMDA application to neuronal cultures. As shown in Fig. 1*B*, treatment of neuronal cultures with lactacystin prevented NMDA-R–dependent Ago2 decrease in dendrites, indicating that Ago2 down-regulation involves the proteasomal pathway. We next repeated this experiment with an alternative mAb against Ago2 to validate our results. With this alternative antibody we obtained the identical result, *i.e.* a significant decrease of Ago2 upon NMDA-R stimulation, which is prevented by pretreatment of neuronal cultures with the proteasome inhibitor lactacystin (Fig. 1*C*).

NMDA-R activation triggers dephosphorylation of Ago2 at Ser-387

Having found that activation of NMDA-Rs promotes proteasome-dependent down-regulation of Ago2 in dendrites, we wanted to shed light onto the underlying signaling pathway. It has been shown that Ago2 protein turnover is influenced by its localization to processing bodies (P-bodies) (33, 35, 43), which are involved in translational repression and RNA decay (44, 45). Phosphorylation of Ago2 at Ser-387 has been reported to promote the accumulation of Ago2 to cytoplasmic granules such as P-bodies and has been shown to increase translational repression by Ago2 (46, 47). We therefore analyzed whether NMDA-R signaling affects the phosphorylation of Ago2 at Ser-387. Neuronal cultures were treated with NMDA, and relative levels of Ser-387–phosphorylated Ago2 (Ago2 pSer-387) and total Ago2 in whole-cell lysates were determined by Western blotting. We observed two bands with the antibody directed against total Ago2, with only the upper band being recognized by the phosphospecific antibody against Ago2 pSer-387 (Fig. 2*A*). To test the specificity of the Ago2 pSer-387 antibody, we incubated the Western blotting PVDF membrane with alkaline phosphatase. As shown in Fig. S3, alkaline phosphatase treatment completely abolishes the Ago2 pSer-387 signal. Importantly, our result from Fig. 2*A* shows that NMDA-R activation leads to a specific decrease of Ser-387–phosphorylated Ago2 when compared with total Ago2 (combined intensity of the upper and lower band). As shown previously by other research groups, Ago2 undergoes multiple post-translational modifications, such as sumoylation, that lead to an increase in molecular weight (48) and, in conjunction with Ser-387 phosphorylation, are most likely responsible for the occurrence of the larger shift for the upper band in the total Ago2 Western blotting.

Next, we wanted to corroborate our Western blotting results and verify with immunofluorescent labeling that the reduction in Ago2 pSer-387 upon NMDA stimulation occurs in dendrites. We observed in NMDA-treated neurons a decrease in dendritic Ago2 pSer-387 in parallel to a decrease in dendritic total Ago2 (Fig. 2*B*). However, the decrease in Ago2 pSer-387 was greater in proportion than the decrease in total Ago2, as indicated by the lower ratio of Ago2 pSer-387 to total Ago2 in dendrites stimulated with NMDA. This result corroborates our initial Western blotting results from Fig. 2*A*.

Our observation that NMDA-R activation leads to a specific reduction of Ser-387–phosphorylated Ago2 could be explained by two different scenarios: (*a*) either NMDA-R activation triggers the degradation of Ser-387–phosphorylated Ago2; or (*b*) NMDA-R activation leads to Ago2 Ser-387 dephosphorylation, and it is the dephosphorylated Ago2 that is preferentially subjected to degradation. To test these two mutually exclusive hypotheses, we incubated neuronal cultures with the proteasome inhibitor lactacystin and analyzed whether we would still observe NMDA-dependent dephosphorylation of Ago2 pSer-387 in the absence of proteasomal degradation. To prevent the theoretical possibility that newly synthesized unphosphorylated Ago2 could affect the ratio of Ago2 pSer-387 to total Ago2, we added the protein synthesis inhibitor cycloheximide to neuronal cultures. Western blot analysis revealed that neurons treated with lactacystin still showed a significant reduction in Ago2 Ser-387 phosphorylation with NMDA-R activation, which was comparable with the reduction seen in neurons not incubated with lactacystin (Fig. 3, *A–C*). However, lactacystin did prevent decrease of total Ago2 protein amount upon NMDA-R activation (Fig. 3*A*), similarly to what we previously observed in dendrites by immunocytochemistry (Fig. 1, *B* and *C*). Furthermore, we tested an alternative proteasome inhibitor, MG132, and obtained the same result as with lactacystin, *i.e.* NMDA-induced reduction of Ago2 protein was blocked by MG132 (Fig. S4). These results indicate that

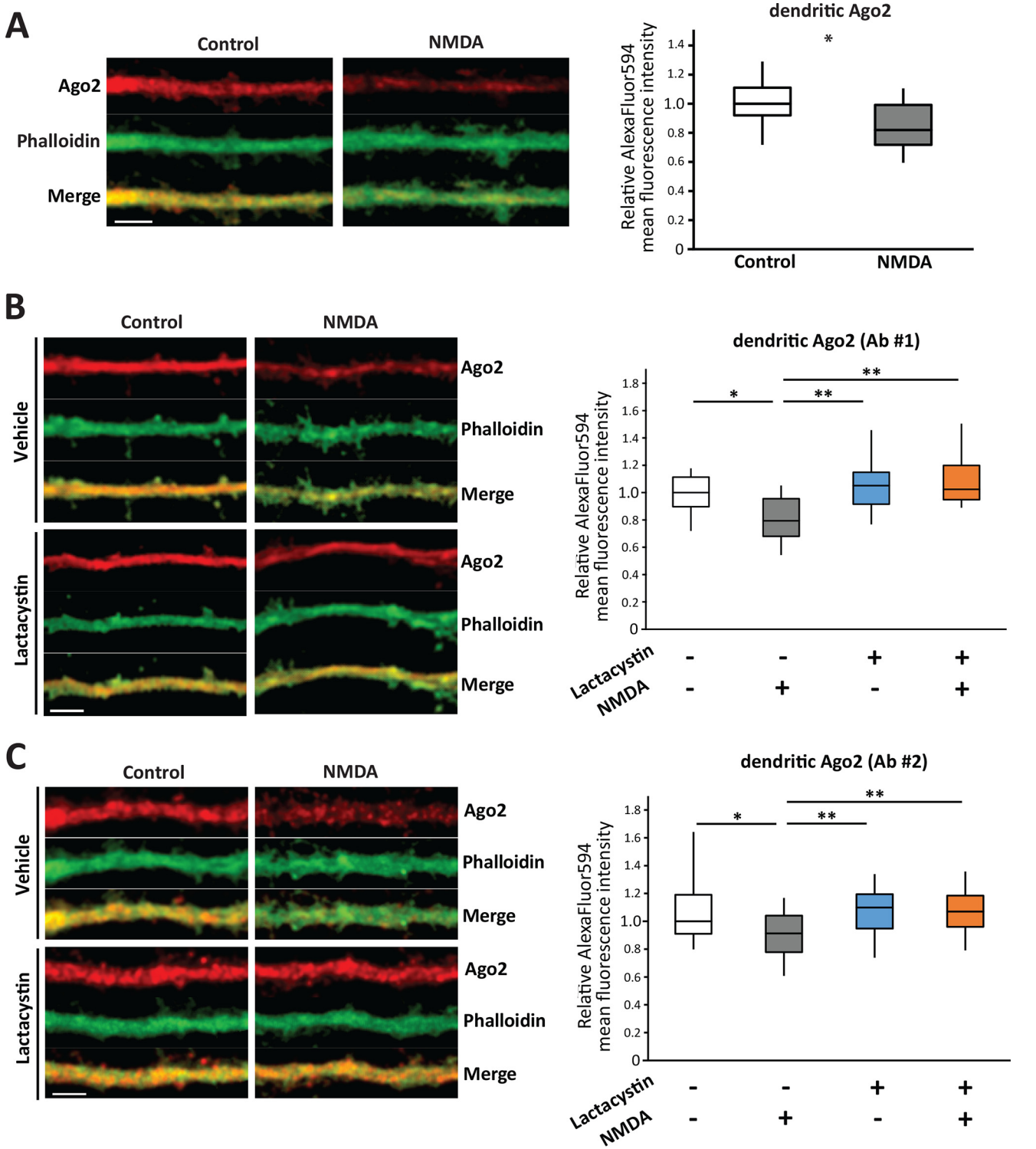

Figure 1. NMDA-R activation leads to a rapid, proteasome-dependent decrease of Ago2 levels in hippocampal neurons. *A*, immunocytochemistry analysis of Ago2 protein (*red*) in dendrites of cultured hippocampal neurons (DIV19) counterstained with phalloidin-FITC (*green*) and treated with or without NMDA (40 μM NMDA, 15 min) prior to fixation. *Left,* representative images of primary dendrite segments. *Right, whisker and box plot* of Ago2 (AlexaFluor594) mean fluorescence intensity of 62.1-μm segments of proximal dendrites in different neurons (results normalized to control condition median; *Control*, $n = 16$; *NMDA*, $n = 19$; two-tailed Mann-Whitney *U* test, *, $p < 0.05$). *B*, immunocytochemistry analysis of Ago2 protein (*red*) with Wako clone 4D2 mAb (*Ab#1*) in dendrites of cultured hippocampal neurons (DIV19) counterstained with phalloidin-FITC (*green*), with or without lactacystin pretreatment (*Lactacystin*; 5 μM, 1 h) and with or without NMDA (40 μM NMDA, 15 min) treatment immediately prior to fixation. Shown is *whisker and box plot* of Ago2 (AlexaFluor594) fluorescence intensity in dendrites (results normalized to control condition median; vehicle, $n = 24$; vehicle + NMDA, $n = 19$; lactacystin, $n = 22$; lactacystin + NMDA, $n = 18$; Kruskal-Wallis test $p = 0.0002$; Dunn's multiple comparisons post-test, *, $p < 0.05$; ** $p < 0.01$). *C*, immunocytochemistry analysis of Ago2 protein (*red*) with a different antibody than in *A*, Abcam ab57113 mAb (*Ab#2*), in dendrites of cultured hippocampal neurons (DIV19) counterstained with phalloidin-FITC (*green*), with or without lactacystin pretreatment (*Lacta.*, 5 μM, 1 h) and with or without NMDA (20 μM, 5 min) treatment immediately prior to fixation. Shown is *whisker and box plot* of Ago2 (AlexaFluor594) mean fluorescence intensity in dendrites (results normalized to control condition median; vehicle, $n = 27$; vehicle + NMDA, $n = 27$; lactacystin, $n = 27$; lactacystin + NMDA, $n = 27$; Kruskal-Wallis test, $p = 0.0018$; Dunn's multiple comparisons post-test, *, $p < 0.05$; **, $p < 0.01$).

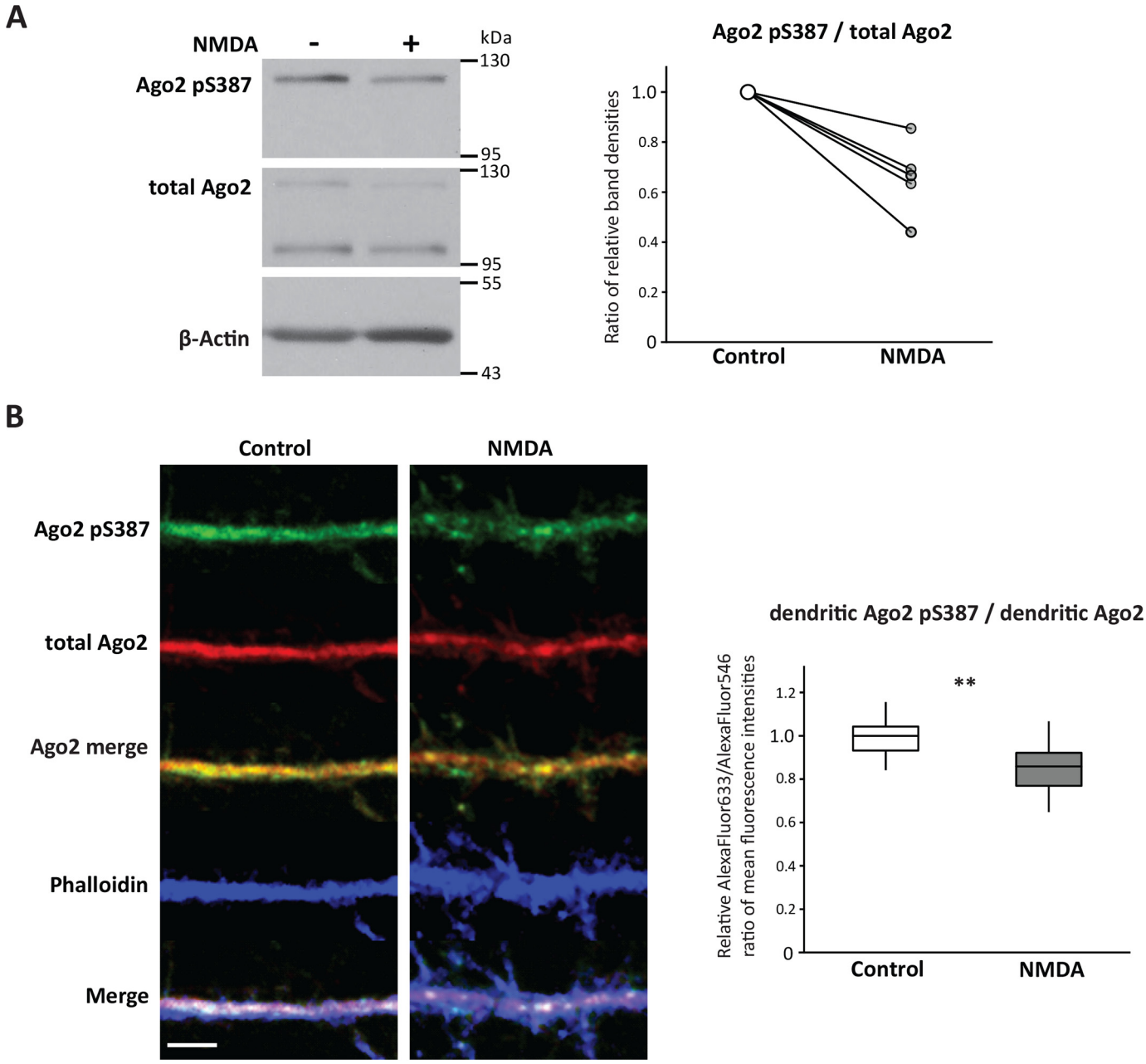

Figure 2. NMDA receptor activation leads to a rapid decrease of Ser-387 phosphorylation in Ago2. *A*, Western blotting of hippocampal neurons (DIV23) treated with or without NMDA (20 μM, 5 min). *Left*, representative image of Ago2 pSer-387 *versus* total Ago2 Western blots (with corresponding β-actin loading control). *Right,* change in Ago2 pSer-387/total Ago2 ratio of paired samples for five independent experiments (each NMDA sample normalized to paired *Control*; one-tailed sign test, $p < 0.05$). *B*, immunocytochemistry analysis of Ago2 pSer-387 protein (*red*) *versus* total Ago2 (*green*) in dendrites of cultured hippocampal neurons (DIV19) counterstained with phalloidin-FITC (*green*), with or without NMDA treatment (40 μM NMDA, 15 min) immediately prior to fixation. Shown is *whisker and box plot* for Ago2 pSer-387/total Ago2 relative ratio of mean fluorescence intensities in dendrites (results normalized to respective control condition median; *Control*, $n = 24$, *NMDA*, $n = 19$; two-tailed Mann-Whitney *U* test; **, $p < 0.01$).

NMDA-R activation induces the dephosphorylation of Ago2 at Ser-387, which occurs independently from Ago2 degradation by the proteasome, suggesting that this dephosphorylation precedes NMDA-R–dependent Ago2 degradation by the proteasome.

Ser-387 phosphorylation-deficient Ago2 is readily degraded upon NMDA-R activation

Although our results so far point toward a link between Ago2 dephosphorylation at Ser-387 and Ago2 degradation upon NMDA-R stimulation, they do not provide direct evidence that the dephosphorylation of Ago2 is a necessary event for the targeted degradation of Ago2. To further elucidate the role of Ago2 Ser-387 phosphorylation in regulating Ago2 turnover, we cloned an eGFP-tagged Ago2 WT construct (Ago2WT) as well as an eGFP-tagged phosphoblock mutant of Ago2 with serine 387 substituted by alanine (Ago2S387A) and an eGFP-tagged phosphomimetic mutant of Ago2 with serine 387 substituted by aspartic acid (Ago2S387D). First, we transfected neuronal cultures with these constructs and analyzed their level of

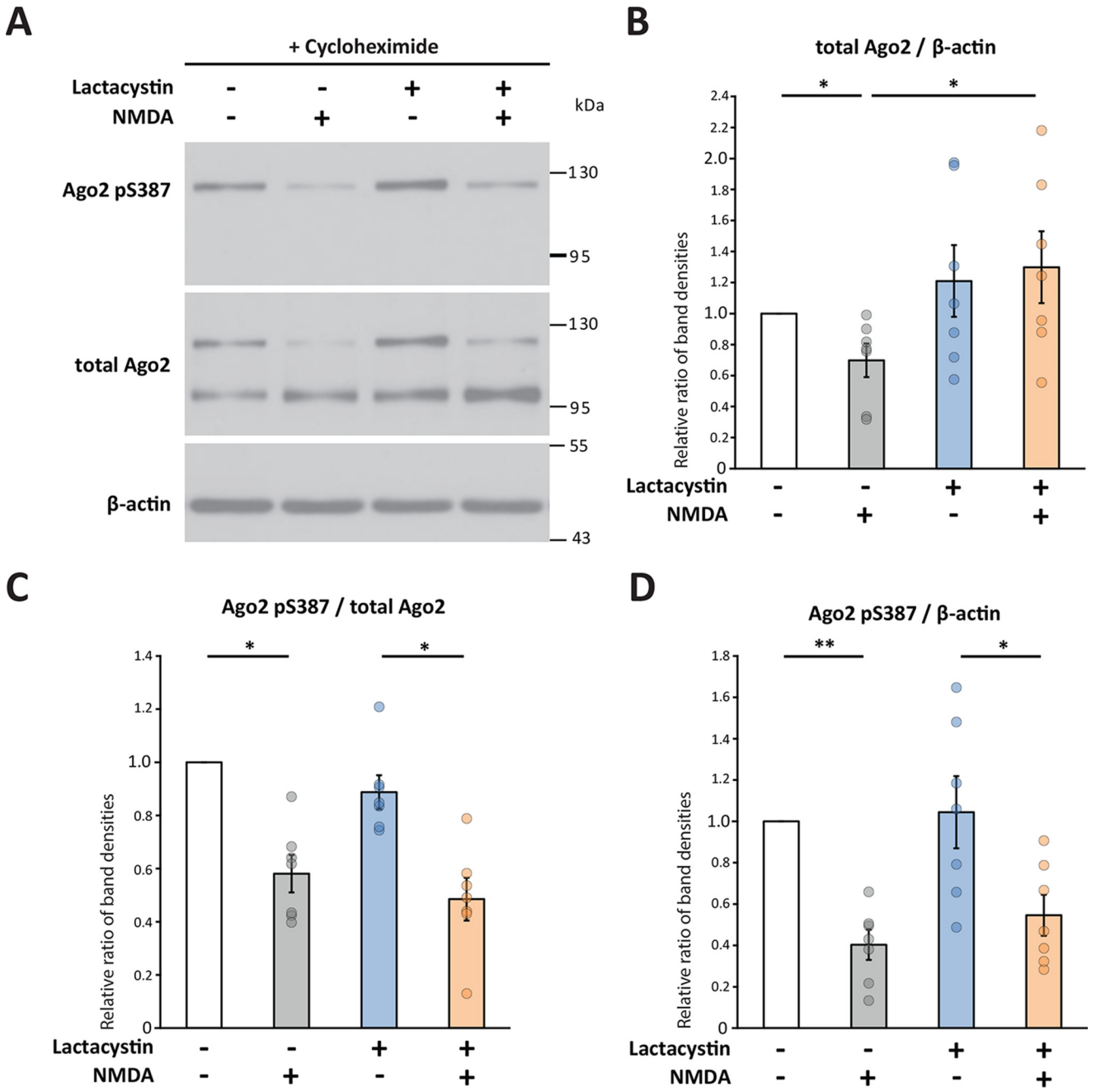

Figure 3. NMDA receptor activation leads to both dephosphorylation of Ago2 Ser-387 and Ago2 degradation. *A*, matched hippocampal neuronal cultures (DIV23) treated with protein synthesis inhibitor cycloheximide (25 μg/ml) and lactacystin (5 μM, 1 h) or vehicle (DMSO) and stimulated with or without NMDA (40 μM NMDA, 15 min). Shown are representative images of Western blotting for Ago2 pSer-387, total Ago2, and β-actin from the same Western blotting membrane (total Ago2 probed after stripping) for series of matched samples. *B*, histogram (mean ± S.E.) of total Ago2 standardized to β-actin; Friedman test overall p value 0.0145. *C*, histogram (mean ± S.E.) of Ago2 pSer-387 standardized to total Ago2; Friedman test overall p value 0.0003. *D*, histogram (mean ± S.E.) of Ago2 pSer-387 standardized β-actin; Friedman test overall p value 0.0017. *B, C,* and *D,* values for series of matched samples normalized to respective control (vehicle only) sample, $n = 7$; Dunn's multiple comparisons post-test, *, $p < 0.05$; **, $p < 0.01$).

expression. As shown in Fig. S5, expression of eGFP- tagged Ago2WT, Ago2S387A, and Ago2S387D caused a 2–3-fold increase in total Ago2 immunostaining compared with eGFP-expressing control neurons. Importantly, the overall expression level of Ago2WT, Ago2S387A, and Ago2S387D did not differ among the different constructs. We next transfected neurons with Ago2WT and tdTomato (a red fluorescent protein to visualize the complete neuronal structure and for standardization of eGFP-Ago2 fluorescence intensity) and tested whether ectopically expressed Ago2WT is regulated in a similar fashion like endogenous Ago2, *i.e.* it is degraded upon NMDA-R activation in a proteasome-dependent manner. Like before with endogenous Ago2, we observed that eGFP-Ago2-WT is decreased in dendrites by NMDA-R stimulation and that this down-regulation is prevented by proteasome inhibition (Fig. 4*A*).

To verify that Ser-387 dephosphorylation is an obligatory step for the proteasome-dependent down-regulation of Ago2

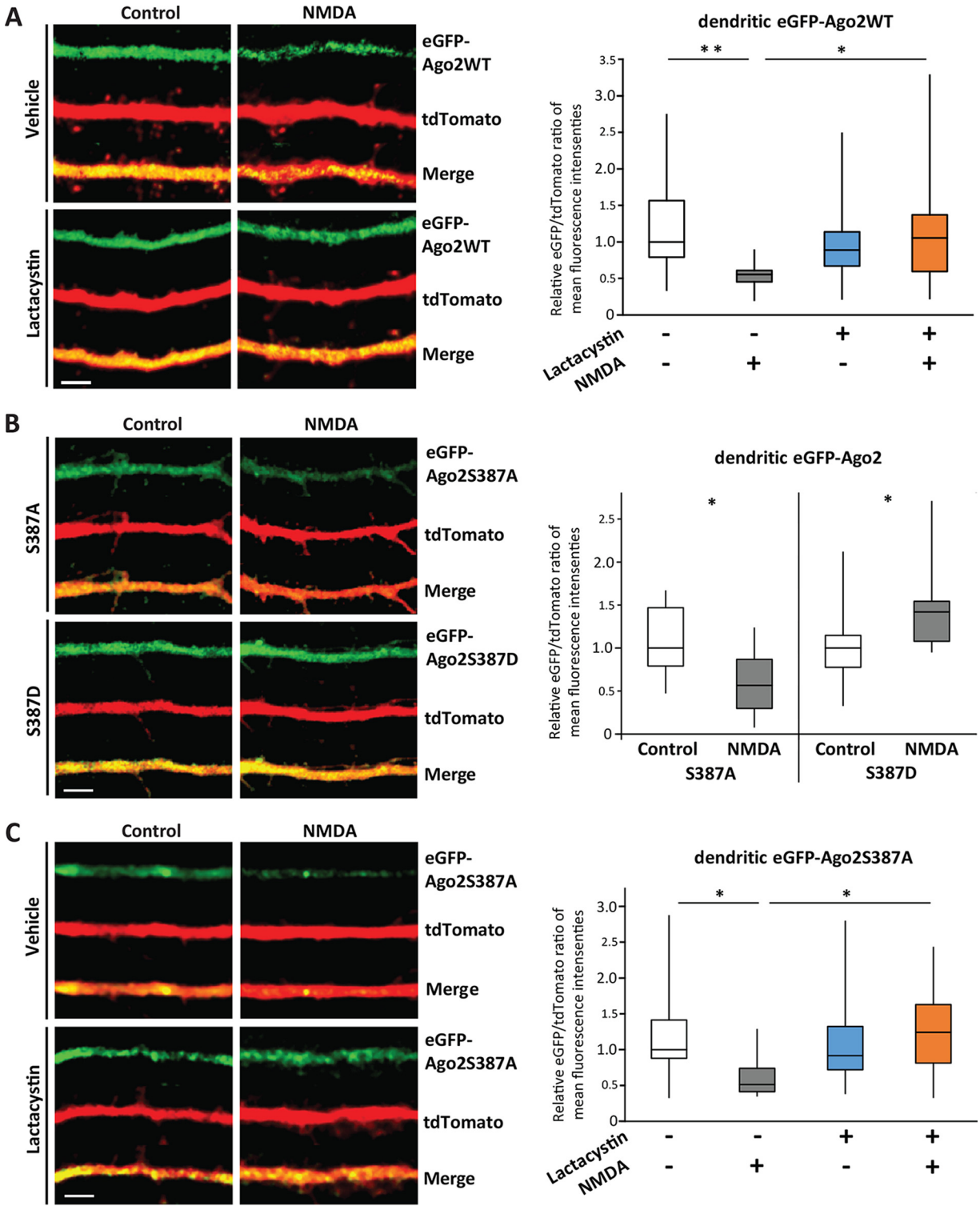

Figure 4. Ago2-S387D phosphomimetic mutant blocks NMDA-induced Ago2 degradation. *A*, analysis of eGFP-Ago2WT in primary dendrites of DIV17 cultured hippocampal neurons, transfected with pEGFP-Ago2WT and pCI-tdTomato, treated with lactacystin (5 μM, 1 h) or vehicle (DMSO) and with or without NMDA treatment (40 μM NMDA, 15 min) prior to fixation. Shown is *whisker and box plot* of relative eGFP-Ago2/tdTomato ratio of mean fluorescence intensities in dendrites (results normalized to control condition median; vehicle, $n = 14$; vehicle + NMDA, $n = 11$; lactacystin, $n = 14$; lactacystin + NMDA, $n = 15$; Kruskal-Wallis test, $p = 0.0278$; Dunn's multiple comparisons post-test, *, $p < 0.05$). *B*, analysis of eGFP-Ago2S387A and eGFP-Ago2S387D in dendrites of DIV15 cultured hippocampal neurons, transfected with pEGFP-Ago2S387A or pEGFP-Ago2S387D and pCI-tdTomato, with or without NMDA treatment prior to fixation (40 μM NMDA, 15 min). Shown is *whisker and box plot* of relative eGFP-Ago2/tdTomato ratio of mean fluorescence intensities in dendrites (results normalized to respective control condition median; S387A control, $n = 17$; S387A NMDA; $n = 15$; two-tailed Mann-Whitney *U* test, *, $p < 0.05$; S387D control, $n = 19$; S387D NMDA, $n = 11$; two-tailed Mann-Whitney *U* test, *, $p < 0.05$). *C*, analysis of eGFP-Ago2S387A in dendrites of DIV17 cultured hippocampal neurons, transfected with pEGFP-Ago2S387A and pCI-tdTomato, treated with lactacystin or vehicle (DMSO) and with or without NMDA treatment (40 μM NMDA, 15 min) prior to fixation. Shown is *whisker and box plot* of relative eGFP-Ago2/tdTomato ratio of mean fluorescence intensities in dendrites (results normalized to control condition median; vehicle, $n = 17$; vehicle + NMDA, $n = 13$; lactacystin, $n = 11$; lactacystin + NMDA, $n = 11$; Kruskal-Wallis test, $p = 0.0110$; Dunn's multiple comparisons post-test, *, $p < 0.05$).

upon NMDA-R activation, we tested whether Ago2 with a phosphomimetic mutation at Ser-387 (Ago2S387D) is protected from NMDA-R–dependent degradation. Hippocampal neurons were transfected with expression vectors for either eGFP-Ago2S387A or eGFP-Ago2S387D and tdTomato. Although the phosphoblock form of Ago2 was down-regulated in dendrites, we observed that the phosphomimetic form was up-regulated upon NMDA treatment (Fig. 4*B*). Although this last result might suggest that the S387D mutant undergoes increased recruitment into stimulated dendrites, it more importantly shows that Ago2 Ser-387 dephosphorylation is a necessary prerequisite for Ago2 proteasomal degradation.

Our results in Figs. 3 and 4*B* suggest that NMDA-R activation induces a two-step process. First, NMDA-R activation causes Ago2 dephosphorylation at Ser-387. Second, NMDA-R activation causes subsequent Ago2 degradation by increasing proteasomal activity. To validate this two-step process, we tested whether Ago2 with a phosphoblock mutation at Ser-387 (S387A) is still subjected to increased proteasomal degradation after NMDA-R activation. eGFP-Ago2S387A and tdTomato were expressed together in hippocampal neurons and treated with NMDA with or without prior incubation with lactacystin. Again, we observed a reduction of Ago2S387A in dendrites upon NMDA-R activation, which is absent in lactacystin-treated neurons (Fig. 4*C*). Taken together, these findings show that dephosphorylation at Ago2 Ser-387 after NMDA-R activation permits the subsequent degradation of unphosphorylated Ago2 by the proteasome.

So far, we found that NMDA-R activation leads to the dephosphorylation and degradation of Ago2 in dendrites. However, in hippocampal neurons, NMDA-Rs are enriched at synapses on dendritic spines (49, 50). We therefore analyzed eGFP-Ago2 turnover in tertiary dendrites where spines are more abundant than in the primary dendrites analyzed so far. The ectopic expression of eGFP-Ago2WT together with tdTomato allowed us to compare the effects of NMDA application on Ago2 levels in spines *versus* dendrites. Similar to dendrites (Fig. 4*A*), we found that eGFP-Ago2 levels are also decreased in spines upon NMDA-R activation (Fig. 5, *A* and *B*). Interestingly, when comparing the turnover of eGFP-Ago2 in spines *versus* dendrites, we observed a greater decrease of Ago2 in spines compared with dendrites after NMDA-R stimulation (Fig. 5, *C* and *D*).

Ago2 Ser-387 dephosphorylation leads to increased spine density and PSD-95 enrichment

Finally, we turned our attention to the physiological consequences of Ago2 Ser-387 phosphorylation in dendrites. Reducing Ago2 phosphorylation at Ser-387 has been shown to decrease miRNA-induced repression of mRNAs (46). Furthermore, several research groups reported that miRNA-dependent translational regulation of local protein expression is associated with synaptogenesis and synaptic plasticity (22–27). Hence, we hypothesized that the NMDA-R–dependent dephosphorylation of Ago2 Ser-387 could be involved in regulating the release of mRNA repression and thereby allowing the local translation of mRNAs in dendrites and spines.

To test whether Ago2 Ser-387 phosphorylation affects spine growth and shape, we expressed Ago2WT, Ago2S387A, or Ago2S387D in cultured hippocampal neurons and quantified dendritic spines on tertiary dendrites. In Ago2WT-expressing neurons, NMDA-R activation was associated with an increase in spine density (Fig. 6*A*). Interestingly, expression of Ago2S387A by itself increased spine density in untreated transfected neurons, and NMDA treatment did not further increase spine density for Ago2S387A-expressing neurons, indicating that blocking Ago2 Ser-387 phosphorylation occludes the effects of NMDA-R stimulation on spine density. In untreated Ago2S387D-expressing neurons, spine density was similar to that of untreated Ago2WT-expressing neurons. However, in contrast to Ago2WT-expressing neurons, NMDA-R activation was not associated with an increase in spine density in neurons expressing Ago2S387D. These results indicate that mimicking Ser-387 phosphorylation of Ago2 blocks the effects of NMDA-R stimulation on spine density. Overall, our results that NMDA-R–dependent spine increase is mimicked by phospho-deficient Ago2 and blocked by phosphomimetic Ago2 support the involvement of Ago2 Ser-387 phosphorylation in modulating NMDA-R–dependent spine growth.

The finding that the expression of Ago2S387A in itself is associated with an increase in total spine density (Fig. 6*A*) prompted us to further analyze whether Ago2 Ser-387 phosphorylation affects spine maturation. Spines are classified based on their shape as mushroom-like, stubby, or thin spines, with mushroom-like spines being the most mature form (51). To verify whether Ago2 Ser-387 phosphorylation has an impact on the occurrence of the different spine types, *i.e.* mushroom, stubby, and thin spines, hippocampal neurons were transfected with either Ago2WT, Ago2S387A, or Ago2S387D (+ tdTomato). We found that mushroom spines are more numerous in neurons expressing Ago2S387A compared with Ago2WT or Ago2S387D, whereas no significant differences in thin and stubby spines could be observed (Fig. 6*B*). Given that mushroom spines are considered to be the most mature form of spines (51), our results suggest that Ago2 Ser-387 dephosphorylation contributes to spine maturation.

An important factor in dendritic spine maturation and excitatory synapse formation is the enrichment of PSD-95 in spines (52, 53). Importantly, Ago2 has been reported to be directly involved in the regulation of PSD-95 mRNA in the dendrites of hippocampal neurons (24). To analyze the possible role of Ago2 Ser-387 phosphorylation in regulating PSD-95 enrichment in spines, hippocampal neurons were transfected with either Ago2WT, Ago2S387A, or Ago2S387D (+ tdTomato), and PSD-95 expression was analyzed by immunocytochemistry. Although the increase in PSD-95 in neurons expressing Ago2S387A compared with AgoWT was not statistically significant, we observed a significant increase in PSD-95 in neurons expressing Ago2S387A compared with neurons expressing phosphomimetic Ago2S387D (Fig. 6*B*, *bottom*).

Taken together, the effects of the phosphoblock mutation of Ago2S387A *versus* phosphomimetic Ago2S387D on dendritic spine density and morphology, as well as on PSD95 enrichment in spines, support the involvement of Ago2 Ser-387 dephosphorylation in spine growth and maturation.

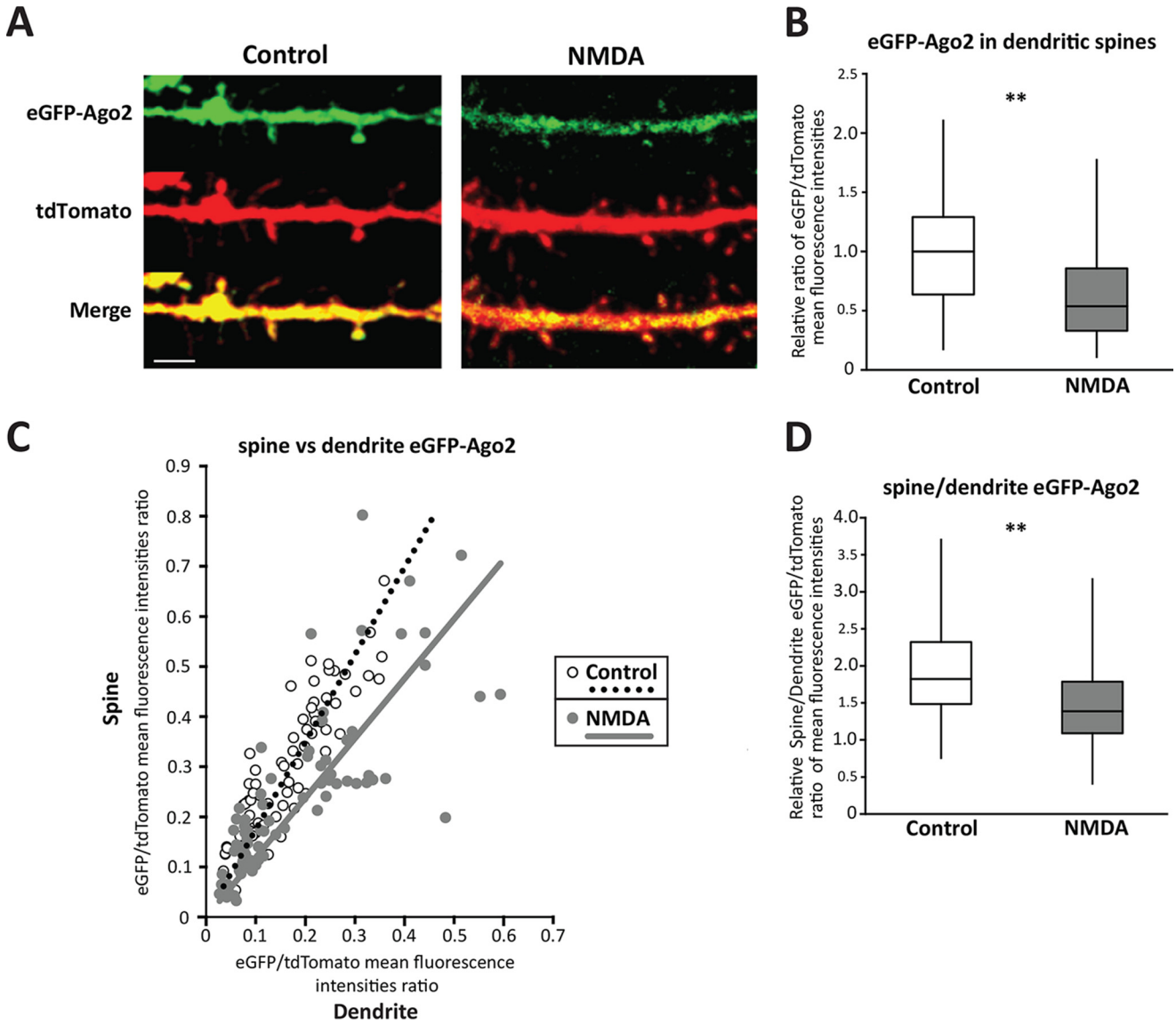

Figure 5. NMDA-induced Ago2 decrease occurs to a greater extent in dendritic spines than in dendrites. *A*, tertiary dendrites of DIV18 cultured hippocampal neurons, transfected with pEGFP-Ago2WT and pCI-tdTomato, treated with or without NMDA (40 μM NMDA, 15 min) prior to fixation. *B*, analysis of eGFP-Ago2 in dendritic spines of tertiary dendrites. Shown is *whisker and box plot* of relative eGFP-Ago2/tdTomato ratio of mean fluorescence intensities in spines (results normalized to control condition median; control, $n = 89$ spines from 10 neurons; NMDA, $n = 75$ spines from 10 neurons; two-tailed Mann-Whitney test, **, $p < 0.01$). *C*, scatter plot of eGFP-Ago2/tdTomato ratio in spines (*vertical axis*) *versus* eGFP-Ago2/tdTomato ratio in corresponding regions of interest (same size and shape) in tertiary dendrites. *Dotted line,* control, linear trend; *gray full line,* NMDA linear trend. *D*, *whisker and box plot* of spine/dendrite eGFP-Ago2/tdTomato ratio (results normalized to control condition median; *control*, $n = 89$ spines from 10 neurons; *NMDA,* $n = 75$ spines from 10 neurons; two-tailed Mann-Whitney test, **, $p < 0.01$).

Discussion

Mature miRNAs associate with AGO proteins to exert their regulatory effects on mRNA translation (12, 20, 21, 44). Several studies have shown that dendritic localization and interaction of Ago2 with components of the miRNA pathway are modulated by neuronal maturation and neuronal activity (22–24, 27, 54–57).

Here, we show that neuronal activity in the form of NMDA-R activation leads to Ago2 dephosphorylation at Ser-387 and proteasome-dependent degradation of Ago2 in dendrites of hippocampal neurons. Furthermore, neuronal expression of a phosphodeficient mutant of Ago2 that blocks phosphorylation of Ser-387 causes an increase in spine density. Overall, our observations support a model (Fig. 7) where NMDA-receptor activation through the regulation of Ago2 turnover contributes to the derepression of mRNAs involved in spine growth and maturation.

NMDA-R–dependent degradation of Ago2

Neuronal activity, especially NMDA-R activation, is known to up-regulate proteasomal activity and turnover of a variety of proteins in dendrites and spines (2–4, 40, 58). A widely accepted view, supported by several lines of evidence, proposes that synaptic activity leads in general to an acute increase in turnover of several mature miRNAs and derepression of their mRNA targets (19, 21, 59–61). Our result that NMDA-R activation causes proteasome-dependent Ago2 degradation therefore provides a mechanistic frame for the local synaptic dere-

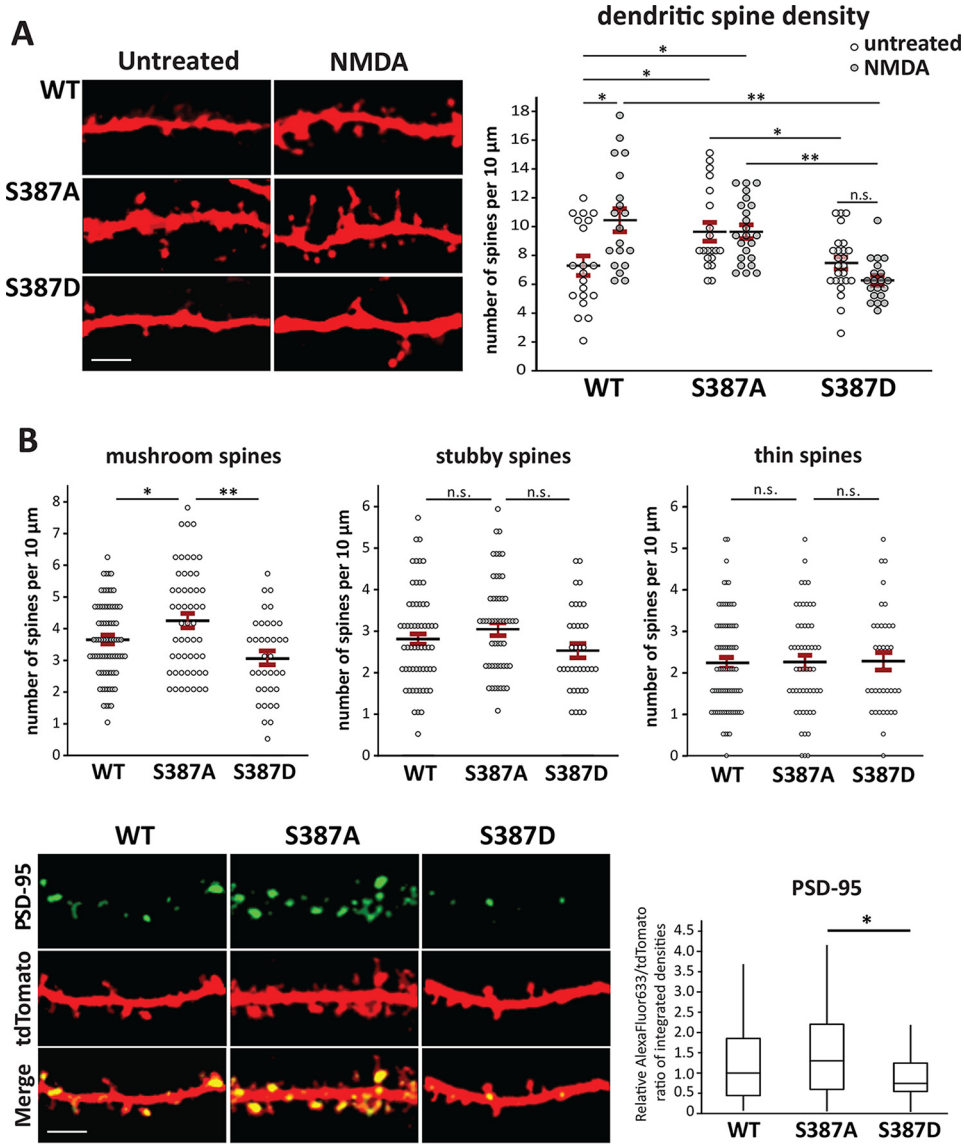

Figure 6. Ago2 Ser-387 phosphorylation affects dendritic spine density and morphology. *A*, dendritic spine density after NMDA treatment (40 μM NMDA, 15 min; + 15-min follow up) of DIV19 cultured hippocampal neurons transfected at DIV15 with pCI-tdTomato and either pEGFP-Ago2WT, pEGFP-Ago2S387A, or pEGFP-Ago2S387D. *Left,* representative images of tertiary dendrites of transfected neurons (tdTomato, *red*). *Right,* spine numbers and analysis of relative spine density for tertiary dendrites (means ± S.E., results normalized to Ago2WT control condition mean; Ago2WT control, $n = 20$ dendrites from 10 neurons; Ago2WT NMDA, $n = 20$ dendrites from 11 neurons; Ago2S387A control, $n = 20$ dendrites from 11 neurons; Ago2S387A NMDA, $n = 23$ dendrites from 11 neurons; Ago2S387D control, $n = 25$ dendrites from 12 neurons; Ago2S387A NMDA, $n = 20$ dendrites from 12 neurons; two-way ANOVA overall p value 0.0041; post-hoc Tukey test *, $p < 0.05$; **, $p < 0.01$). *B*, DIV18 cultured hippocampal neurons, transfected at DIV14 with pCI-tdTomato (*red*) and either pEGFP-Ago2WT, pEGFP-Ago2S387A, or pEGFP-Ago2S387D were subjected to spine analysis and immunocytochemistry analysis for PSD-95. *Top,* spine numbers and analysis of spine density for each spine type: *mushroom*, *stubby* and *thin spines* (means ± S.E., results normalized to Ago2WT mean; Ago2WT, $n = 78$ dendrites from 29 neurons; Ago2S387A, $n = 53$ dendrites from 20 neurons; Ago2S387D, $n = 36$ dendrites from 13 neurons). *Mushroom spines* (*left panel*), one-way ANOVA, $p = 0.0005$; *stubby spines* (*center panel*), one-way ANOVA, $p = 0.09$; *thin spines* (*right panel*), one-way ANOVA, $p = 0.99$; post-hoc Tukey tests; *, $p < 0.05$, **, $p < 0.01$; *n.s.*, not significant). *Bottom left*, representative images of tertiary dendrites of transfected neurons (tdTomato, *red*) labeled for PSD-95 (*green*). *Bottom right,* analysis of differences in PSD-95 expression, using PSD-95 (AlexaFluor633) fluorescent density standardized to tdTomato fluorescent density in the same region of interest (results are normalized to Ago2WT median; Ago2WT, $n = 78$ dendrites from 29 neurons; Ago2S387A, $n = 53$ dendrites from 20 neurons; Ago2S387D, $n = 36$ dendrites from 13 neurons; Kruskal-Wallis test $p = 0.0416$; Dunn's multiple comparisons post-test, *, $p < 0.05$).

pression of miRNA-targeted transcripts as well as miRNA turnover in neurons.

In addition, the activity- and proteasome-dependent turnover of Ago2, as described here, is similar to the degradation of MOV10 (an Ago2-interacting protein that is degraded after NMDA-R activation) and FMRP (a RNA-binding protein that also interacts with Ago and is degraded after mGluR activation) in cortical and hippocampal neurons, as reported previously (26, 62). Importantly, MOV10 and FMRP have both been found to regulate Ago2 association to mRNAs (62, 63). Taken together, these findings and our results suggest a common scheme where neuronal activity regulates the dendritic miRNA pathway through proteasomal degradation of its key effector proteins.

NMDA-R–dependent dephosphorylation of Ago2

Ago2 Ser-387 phosphorylation favors Ago2 localization to processing bodies (P-bodies), *i.e.* to cytoplasmic granules where

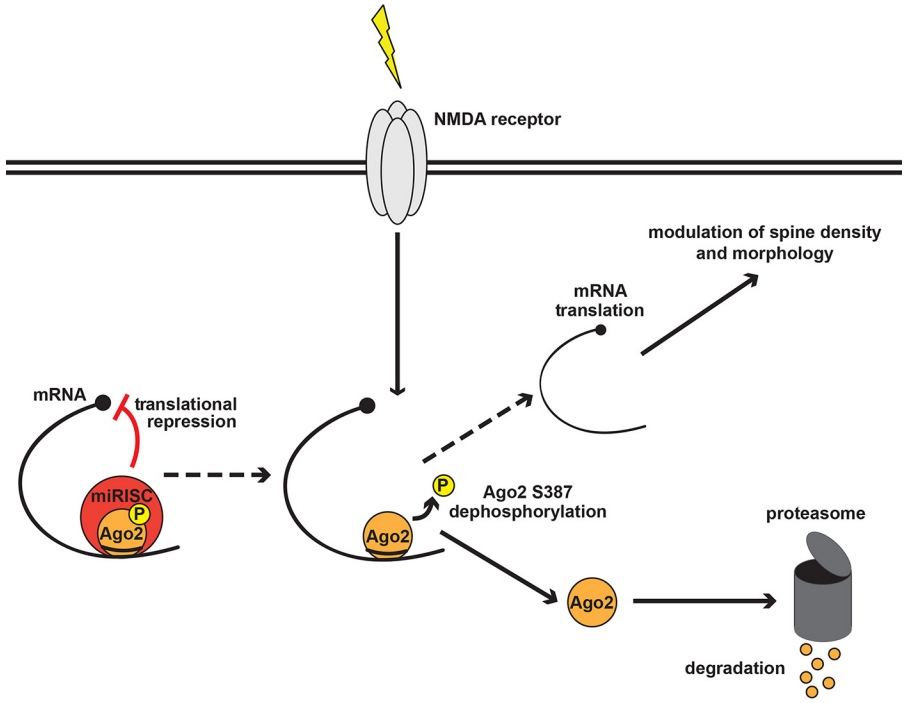

Figure 7. Proposed model for the role of NMDA-R–dependent Ago2 Ser-387 dephosphorylation and Ago2 degradation in modulating dendritic spine density and morphology. Ago2 as part of the microRNA-induced silencing complex (miRISC) represses the translation of certain mRNAs. Acute NMDA-R activation induces dephosphorylation of Ago2 at Ser-387 and degradation of Ago2 via the proteasome (through a process that most likely involves elevated NMDA-R–dependent calcium influx). Ago2 dephosphorylation and subsequent degradation is then allowing the translation of mRNAs involved in the formation of new dendritic spines and the maturation or stabilization of existing spines.

miRNA-targeted mRNAs are stored or degraded (46, 47). Therefore, our observation that Ago2 Ser-387 is dephosphorylated upon NMDA-R activation (Fig. 3) is in line with findings that neuronal activity, NMDA-R activation in particular, leads to acute disassembly of dendritic P-bodies and release of Ago2 (54, 55). Dephosphorylation of Ago2 Ser-387 has also been shown to reduce miRNA-induced repression of mRNAs (46). Derepression of miRNA-targeted mRNAs involves in general the dissociation of Ago2 from these mRNAs and may lead to the unloading of Ago2 from its miRNAs (20, 21). The pool of Ago2 that is unloaded of its mRNA and/or miRNA is then preferentially targeted for degradation (33, 64). In accordance with these results, we find that dephosphorylation of Ago2 at Ser-387 after NMDA-R activation is associated with increased Ago2 degradation. Two possible mechanisms could account for this effect as follows: either the dephosphorylation of Ser-387 is by itself sufficient to target Ago2 for degradation or the dissociation of Ago2 from RNA in consequence to Ser-387 dephosphorylation renders Ago2 vulnerable to degradation.

Finally, our findings add Ago2 Ser-387 phosphorylation in neurons to a growing number of post-translational modifications of Ago2 that regulate its turnover in non-neuronal cells (20, 33), like the phosphorylation of tyrosine 393 and the sumoylation of lysine 402 that have been shown to also regulate miRNA loading and stability of Ago2 (48, 65, 66). Given the larger molecular weight of phosphorylated Ago2 in Fig. 3, it seems plausible that additional modifications, like sumoylation of Ago2, occur in neurons. However, the role of these additional modifications in regulating Ago2 stability or function in neurons after NMDA-R activation remains unclear.

Modulation of dendritic spines by Ago2 dephosphorylation

Dendritic spines constitute postsynaptic compartments that are composed of an intricate network of scaffolding proteins. During development and synaptic plasticity, changes in spine number and shape are highly dependent on local dendritic protein translation (5, 67). The importance of the miRNA pathway in regulating local mRNA translation in dendrites is well established (6–8, 21), and many miRNAs have been found to impact dendritic morphology (16, 59, 60, 68–71). In accordance with the important role of the miRNA pathway in synaptic maturation and plasticity, we find that the expression of Ago2 with a phosphoblock or a phosphomimetic mutation at Ser-387 impacts dendritic spine density (Fig. 6*A*).

Apart from dendritic spine morphology, we find that neurons expressing Ago2S387A display a synaptic PSD95 enrichment compared with Ago2S387D-expressing cells. PSD-95 is a marker for synaptic maturation (72–74), playing an important role in concentrating glutamate receptors at synapses (52). The PSD-95 mRNA undergoes localized translation in dendrites (67) and was shown to be regulated by Ago2/miRNA-125a in conjunction with FMRP in dendrites (24).

Taken together, our results link NMDA-induced Ago2 Ser-387 dephosphorylation to increased spine density and maturation. Given that proteasomal degradation of MOV10 (an Ago2 interaction partner) is, like Ago2, regulated through NMDA-R activity (26), it appears that NMDA-R–dependent proteasomal degradation of components of the miRNA pathway constitutes an important element for derepression of dendritic mRNAs and local protein synthesis triggered by synaptic activity. Our

findings therefore contribute to an emerging picture where activity-dependent turnover of translational regulators is intimately linked to activity-dependent mRNA translation (26, 75–78). Ultimately, this relationship may offer an explanation as to how proteasome activation is linked to protein synthesis in the context of changes in structural plasticity (38) as well as in long-term memory formation (58, 79).

Materials and methods

DNA constructs

pEGFP-Ago2WT was cloned by inserting human Ago2 from pcDNA3-myc-Ago2 (31) into the pEGFP-C2 vector (Clontech). pEGFP-Ago2S387A and pEGFP-Ago2S387D were generated by PCR site-directed mutagenesis of pEGFP-Ago2WT (tagging with GFP followed a similar approach as described previously (22, 80)).

For S387A, mutagenic primers, 5′-GCAAATTGATGCGAAGTGCAGCTTTCAACACAGATCCATCCATACGTCCG-3′ and 5′-CGGACGTATGGATGGATCTGTGTTGAAAGCTGCACTTCGCATCAATTTGC-3′, were used. For S387D mutagenic primers, 5′-GCAAATTGATGCGAAGTGCAGATTTCAACACAGATCCATACGTCCG-3′ and 5′-CGGACGTATGGATCTGTGTTGAAATCTGCACTTCGCATCAATTTGC-3′ were used.

Animals

The animal protocol (permit no. 17-139) followed the guidelines of the "Comité de Déontologie de l'Expérimentation sur les Animaux" (CDEA) of the Université de Montréal.

Primary neuronal cultures

Hippocampi from E18 to E19 Sprague-Dawley rats were digested in trypsin (0.25%) and mechanically dissociated. Cells were plated onto poly-D-lysine (PDL)–coated 6-well (35 mm) dishes at high density ($2–3 \times 10^5$ cells/ml) for Western blotting experiments and onto PDL/laminin-coated glass coverslips (12-mm round Corning BioCoat Cellware) in 24-well plates at low density ($7–8 \times 10^4$ cells/ml) for imaging experiments. Cultures were maintained in Neurobasal medium with 2% B27 supplement and 0.5 mM GlutaMAX supplement (Gibco), with initially 2% FBS (HyClone), at 37 °C and 5% CO_2. At 3 days *in vitro* (DIV3), for high-density cultures, and DIV4, for low-density cultures, half of the media was replaced with media without FBS and with cytosine-β-D-arabinofuranoside (Ara-C, 2.5 μM) to inhibit glial proliferation. Subsequently, a third to half of the media was replaced without FBS every 4–7 days, depending on culture density and experimental time points.

Drugs and treatments

For all treatments, neurons were incubated at 37 °C, 5% CO_2 in conditioned media with all drugs and other substances added with fresh maintenance media. In initial experiments examining the effects of NMDA-R activation on Ago2 turnover in dendrites (Fig. 1*C*) and on Ago2 Ser-387 phosphorylation (Fig. 2*A*), NMDA (Sigma) was applied at 20 μM (for 5 min). However, for ectopically expressed Ago2 (eGFP-Ago2WT), we found that a stronger and longer stimulation, *i.e.* 40 μM NMDA for 15 min, would lead to more robust/significant effects. Therefore, all other experiments requiring NMDA incubation were performed with 40 μM NMDA for 15 min. In most cases, neurons were fixed or lysed immediately following stimulation. However, for some experiments (Figs. 2*A*, 3, and 6*A*), neurons were washed with media and incubated for an additional 15 min to increase time-dependent effects of NMDA treatment. To inhibit proteasomal degradation, lactacystin (5 μM; Cayman Chemicals and AdipoGen) was applied an hour before NMDA-R stimulation. For the experiments in Fig. 3, we added the protein synthesis inhibitor cycloheximide (25 μg/ml, Acros Organics) to neuronal cultures to prevent the theoretical possibility that newly synthesized Ago2 could affect total Ago2 levels.

Fixation and immunocytochemistry/immunofluorescence

After treatment, neurons were immediately fixed with cold 4% paraformaldehyde (PFA) in PBS with 5 mM $MgCl_2$ for 10 min and additionally in 2% PFA in PBS for 10 min at room temperature.

For immunofluorescence labeling, cells were permeabilized and blocked in 0.2% Triton X-100 and 3% goat serum or 5% BSA in TBS for 20 min at room temperature. Neurons were then incubated with primary antibodies at 1:200 to 1:400 concentrations in TBS with 0.2% Tween 20 and 1.5% goat serum or 2.5% BSA for 1–2 h at room temperature or overnight at 4 °C. Secondary antibodies were applied at 1:100 to 1:300 dilution in TBS with 0.2% Tween.

Indirect immunofluorescent labeling was performed with the following primary antibodies: for (total) Ago2, mouse monoclonal Wako catalog no. 014-22023 (RRID: AB_1106837; Figs. 1, *A* and *B,* and 2*B*) or mouse monoclonal Abcam catalog no. ab57113 (RRID: AB_2230916; Fig. 1*C*); for Ago2 pSer-387, rabbit polyclonal EMC Biosciences catalog no. AP5291 (RRID: AB_2571732); for PSD-95, mouse monoclonal ThermoFisher Scientific catalog no. MA1-046 (RRID: AB_2092361). Secondary antibodies were conjugated with AlexaFluor 488, 546, 594, or 633 (ThermoFisher Scientific). Filamentous actin (F-actin) was stained with phalloidin conjugated to FITC (phalloidin-FITC; Sigma).

Transfections

Hippocampal neuronal cultures grown on coverslips (DIV14/15) were transfected with pCI-tdTomato and pEGFP-Ago2 constructs using Lipofectamine 2000 (Invitrogen) and then transferred to conditioned media without Lipofectamine for 2–3 days (DIV16–19) before treatment and fixation.

Image acquisition and analysis

Image acquisition was performed with an Olympus Fluoview-1000 argon and diode laser-scanning confocal microscope equipped with a Plan-Apo ×60 oil objective (numerical aperture, 1.42). Confocal aperture and z-step size were adjusted automatically through the confocal microscopy platform Olympus Fluoviewer for optimal quantitative imaging of the fluorophores employed in each experiment. For experiments employing the same combination of fluorophores, confocal aperture and z-step size were the same. For each experimental

set, acquisition settings (laser intensity and scan speed) and detector settings (photomultiplier levels, digital gain, and offset) were tested to optimize the quantitative aspect of the signal (at the single z-slice level), to avoid signal saturation or nondetection, oversampling or undersampling, and excessive background and noise. Importantly, all settings, manually or automatically adjusted, were kept constant within an experimental set.

Quantitative analysis of endogenous Ago2 immunolabeling was performed on averaged z-stacks without any image manipulation or enhancement. Quantification of eGFP-Ago2 constructs was performed on summed z-stacks to which background subtraction (automatic, rolling ball, ImageJ) was applied. For quantification of PSD-95 (Fig. 6*B*), thresholding prior to image quantification was used to select double-positive pixels tdTomato and PSD-95 to account for labeling of transfected neurons only.

For quantification of Ago2 in dendrites with immunofluorescence labeling or eGFP fusion constructs, the dendrite appearing to be the most prominent was identified, and a segmented line (*i.e.* continuous with bifurcation points) was drawn manually (ImageJ) for each neuron. To ensure unbiased analysis, the segmented line (for the line plot) was drawn with images only displaying the channel corresponding to the dendritic marker employed (phalloidin for immunolabeled neurons; tdTomato for transfected neurons), with the experimenter being blinded to (*a*) the channel corresponding to labeled or tagged Ago2 and (*b*) to the experimental condition (*e.g.* control *versus* NMDA treatment).

The line plot started at the base of the dendrite (border to the soma) and followed closely the center of the dendrite. Once the line was drawn in the channel corresponding to the dendritic marker, the experimenter added the channel corresponding to labeled or tagged Ago2 to the image to measure fluorescence intensity values in each channel using a line plot function (in Olympus Fluoviewer or ImageJ softwares). All line plots were cut off at a uniform length (300 or 400 pixels, depending on experiments), and the fluorescence intensity was averaged for the retained segments. For quantification of eGFP-Ago2 levels, mean eGFP fluorescence intensity was standardized by the corresponding mean tdTomato fluorescence intensity. The obtained values were then compiled and subjected to statistical analysis (followed by the experimenter not blinded to the experimental condition of the different groups).

For quantification of eGFP-Ago2 in dendritic spines (Fig. 5), images of secondary and tertiary dendrites were acquired. The eGFP/tdTomato ratio of mean fluorescence intensities was measured for each spine individually and matched to an equivalent region of interest (same shape and size) at the base of the spine in the dendrite.

For dendritic spine density and morphology analysis (Fig. 6), images of tertiary dendrites were acquired. Spines were counted in regions of constant length (19.2 μm) along the dendrite (using the tdTomato fluorescent signal to identify dendrites and spines). Spine counts are illustrated in Fig. 6, *A* and *B*, as the number of spines per 10 μm, *i.e.* counted number of spines per 19.2 μm was then converted to number of spines per 10 μm. Spines were visually categorized in three groups: stubby, thin, or mushroom-like.

Western blotting

Immediately prior to lysis, cultures were washed once with ice-cold PBS with 5 mM $MgCl_2$ and 50 μM APV, and then with ice-cold plain PBS. Whole-cell extracts were obtained by scraping cells in denaturing lysis buffer (1% SDS TBS; 200 μl per 35-mm well) and boiling samples at 95 °C for 10 min. Lysates were centrifuged in a tabletop centrifuge for 15 min, and the supernatant was collected. For loading sample preparation, lysates were diluted with an equal volumes of 2× Laemmli buffer (10% β-mercaptoethanol) and boiled at 100 °C for 5 min. Samples were loaded onto 10% SDS-PAGE for electrophoresis and transferred to PVDF membranes. Membranes were blocked in 5% BSA in TBS 0.2% Tween (1 h at room temperature). To analyze Ago2 Ser-387 phosphorylation (Figs. 2*A* and 3), membranes were first incubated with Ago2 pSer-387 rabbit polyclonal antibody (EMC Biosciences catalog no. AP5291, RRID:AB_2571732), diluted 1:1000 in blocking buffer, at 4 °C overnight, followed by incubation with peroxidase-conjugated anti-rabbit IgG (Rockland catalog no. 18-8816-33, RRID: AB_469529) and ECL (GE Healthcare). Afterward, membranes were stripped and probed for total Ago2. For total Ago2 quantification, membranes were incubated with Ago2 mouse mAb (Abcam catalog no. ab57113, RRID: AB_2230916), diluted 1:1000 in blocking buffer, at 4 °C overnight, followed by incubation with peroxidase-conjugated anti-mouse IgG (ThermoFisher Scientific catalog no. 31430, RRID:AB_228307) and ECL. β-Actin mouse mAb conjugated with peroxidase (Sigma catalog no. A2228, RRID: AB_476697) was used as loading control.

Data representation and statistics

Data sets for quantitative fluorescence analysis did not exhibit normal distribution. Therefore, to determine whether differences between datasets were statistically significant, the following nonparametric tests were employed: Mann-Whitney *U* test for experiments with two experimental conditions, and Kruskal-Wallis test (nonparametric ANOVA) with Dunn's multiple comparisons post-test for experiments with more than two experimental conditions. The results for quantitative fluorescence analysis are represented nonparametrically with whisker and box plots (Figs. 1, 2*B*, 4, 5, and 6*B*). The rectangular box represents the range between the 1st quartile and the 3rd quartile. The median is represented as a horizontal line within the box. The whiskers represent the minimum, and the maximum and should not be confused with standard error of the mean or standard deviation. For visual simplicity and comparison purposes, all values for different treatments within an experiment were standardized to the median value of their respective control group.

For analysis of spine density (Fig. 6), the datasets exhibited normal distribution, allowing the use of standard one-way and two-way ANOVA followed by post-hoc Tukey test. For Western blot analysis, experiments were executed in a paired or matched design (*i.e.* independent sets of experiments with each set having its corresponding untreated control), and the obtained densitometric values of each sample were normalized

by their respective control. Hence, the following nonparametric tests were used: a one-tailed sign test for paired samples subjected to two experimental conditions (Fig. 2*A*), and a Friedman test with Dunn's multiple comparisons post-test for matched samples with four conditions (Fig. 3).

Author contributions—N. P.-I. data curation; N. P.-I. formal analysis; N. P.-I. writing-original draft; J. B. conceptualization; J. B. supervision; J. B. writing-review and editing.

Acknowledgments—We thank Drs. DiCristo and Araya for critical comments. We also thank Catherine Bourgeois for technical expertise.

References

1. Cohen, L. D., Zuchman, R., Sorokina, O., Müller, A., Dieterich, D. C., Armstrong, J. D., Ziv, T., and Ziv, N. E. (2013) Metabolic turnover of synaptic proteins: kinetics, interdependencies and implications for synaptic maintenance. *PLoS ONE* **8,** e63191 CrossRef Medline
2. Hanus, C., and Schuman, E. M. (2013) Proteostasis in complex dendrites. *Nat. Rev. Neurosci.* **14,** 638–648 CrossRef Medline
3. Alvarez-Castelao, B., and Schuman, E. M. (2015) The regulation of synaptic protein turnover. *J. Biol. Chem.* **290,** 28623–28630 CrossRef Medline
4. Rosenberg, T., Gal-Ben-Ari, S., Dieterich, D. C., Kreutz, M. R., Ziv, N. E., Gundelfinger, E. D., and Rosenblum, K. (2014) The roles of protein expression in synaptic plasticity and memory consolidation. *Front. Mol. Neurosci.* **7,** 86 Medline
5. Ho, V. M., Lee, J. A., and Martin, K. C. (2011) The cell biology of synaptic plasticity. *Science* **334,** 623–628 CrossRef Medline
6. Weiss, K., Antoniou, A., and Schratt, G. (2015) Non-coding mechanisms of local mRNA translation in neuronal dendrites. *Eur. J. Cell Biol.* **94,** 363–367 CrossRef Medline
7. Jung, H., Gkogkas, C. G., Sonenberg, N., and Holt, C. E. (2014) Remote control of gene function by local translation. *Cell* **157,** 26–40 CrossRef Medline
8. Holt, C. E., and Schuman, E. M. (2013) The central dogma decentralized: new perspectives on RNA function and local translation in neurons. *Neuron* **80,** 648–657 CrossRef Medline
9. Darnell, R. B. (2013) RNA protein interaction in neurons. *Annu. Rev. Neurosci.* **36,** 243–270 CrossRef Medline
10. Pasquinelli, A. E. (2015) MicroRNAs: heralds of the noncoding RNA revolution. *RNA* **21,** 709–710 CrossRef Medline
11. Ebert, M. S., and Sharp, P. A. (2012) Roles for microRNAs in conferring robustness to biological processes. *Cell* **149,** 515–524 CrossRef Medline
12. Jonas, S., and Izaurralde, E. (2015) Towards a molecular understanding of microRNA-mediated gene silencing. *Nat. Rev. Genet.* **16,** 421–433 CrossRef Medline
13. Filipowicz, W., and Sonenberg, N. (2015) The long unfinished march towards understanding microRNA-mediated repression. *RNA* **21,** 519–524 CrossRef Medline
14. Iwakawa, H. O., and Tomari, Y. (2015) The functions of microRNAs: mRNA decay and translational repression. *Trends Cell Biol.* **25,** 651–665 CrossRef Medline
15. Pasquinelli, A. E. (2012) MicroRNAs and their targets: recognition, regulation and an emerging reciprocal relationship. *Nat. Rev. Genet.* **13,** 271–282 CrossRef Medline
16. Ye, Y., Xu, H., Su, X., and He, X. (2016) Role of MicroRNA in governing synaptic plasticity. *Neural Plast.* **2016,** 4959523 Medline
17. Olde Loohuis, N. F., Kos, A., Martens, G. J., Van Bokhoven, H., Nadif Kasri, N., and Aschrafi, A. (2012) MicroRNA networks direct neuronal development and plasticity. *Cell. Mol. Life Sci.* **69,** 89–102 CrossRef Medline
18. Qureshi, I. A., and Mehler, M. F. (2012) Emerging roles of non-coding RNAs in brain evolution, development, plasticity and disease. *Nat. Rev. Neurosci.* **13,** 528–541 CrossRef Medline
19. Siegel, G., Saba, R., and Schratt, G. (2011) MicroRNAs in neurons: manifold regulatory roles at the synapse. *Curr. Opin. Genet. Dev.* **21,** 491–497 CrossRef Medline
20. Meister, G. (2013) Argonaute proteins: functional insights and emerging roles. *Nat. Rev. Genet.* **14,** 447–459 CrossRef Medline
21. Krol, J., Loedige, I., and Filipowicz, W. (2010) The widespread regulation of microRNA biogenesis, function and decay. *Nat. Rev. Genet.* **11,** 597–610 CrossRef Medline
22. Antoniou, A., Baptista, M., Carney, N., and Hanley, J. G. (2014) PICK1 links Argonaute 2 to endosomes in neuronal dendrites and regulates miRNA activity. *EMBO Rep.* **15,** 548–556 CrossRef Medline
23. Pai, B., Siripornmongcolchai, T., Berentsen, B., Pakzad, A., Vieuille, C., Pallesen, S., Pajak, M., Simpson, T. I., Armstrong, J. D., Wibrand, K., and Bramham, C. R. (2014) NMDA receptor-dependent regulation of miRNA expression and association with Argonaute during LTP *in vivo*. *Front. Cell. Neurosci.* **7,** 285 Medline
24. Muddashetty, R. S., Nalavadi, V. C., Gross, C., Yao, X., Xing, L., Laur, O., Warren, S. T., and Bassell, G. J. (2011) Reversible inhibition of PSD-95 mRNA translation by miR-125a, FMRP phosphorylation, and mGluR signaling. *Mol. Cell* **42,** 673–688 CrossRef Medline
25. Edbauer, D., Neilson, J. R., Foster, K. A., Wang, C. F., Seeburg, D. P., Batterton, M. N., Tada, T., Dolan, B. M., Sharp, P. A., and Sheng, M. (2010) Regulation of synaptic structure and function by FMRP-associated microRNAs miR-125b and miR-132. *Neuron* **65,** 373–384 CrossRef Medline
26. Banerjee, S., Neveu, P., and Kosik, K. S. (2009) A coordinated local translational control point at the synapse involving relief from silencing and MOV10 degradation. *Neuron* **64,** 871–884 CrossRef Medline
27. Lugli, G., Larson, J., Martone, M. E., Jones, Y., and Smalheiser, N. R. (2005) Dicer and eIF2c are enriched at postsynaptic densities in adult mouse brain and are modified by neuronal activity in a calpain-dependent manner. *J. Neurochem.* **94,** 896–905 CrossRef Medline
28. Carmell, M. A., Xuan, Z., Zhang, M. Q., and Hannon, G. J. (2002) The Argonaute family: tentacles that reach into RNAi, developmental control, stem cell maintenance, and tumorigenesis. *Genes Dev.* **16,** 2733–2742 CrossRef Medline
29. Sasaki, T., Shiohama, A., Minoshima, S., and Shimizu, N. (2003) Identification of eight members of the Argonaute family in the human genome. *Genomics* **82,** 323–330 CrossRef Medline
30. Valdmanis, P. N., Gu, S., Schüermann, N., Sethupathy, P., Grimm, D., and Kay, M. A. (2012) Expression determinants of mammalian argonaute proteins in mediating gene silencing. *Nucleic Acids Res.* **40,** 3704–3713 CrossRef Medline
31. Liu, J., Carmell, M. A., Rivas, F. V., Marsden, C. G., Thomson, J. M., Song, J. J., Hammond, S. M., Joshua-Tor, L., and Hannon, G. J. (2004) Argonaute2 is the catalytic engine of mammalian RNAi. *Science* **305,** 1437–1441 CrossRef Medline
32. Meister, G., Landthaler, M., Patkaniowska, A., Dorsett, Y., Teng, G., and Tuschl, T. (2004) Human Argonaute2 mediates RNA cleavage targeted by miRNAs and siRNAs. *Mol. Cell* **15,** 185–197 CrossRef Medline
33. Jee, D., and Lai, E. C. (2014) Alteration of miRNA activity via context-specific modifications of Argonaute proteins. *Trends Cell Biol.* **24,** 546–553 CrossRef Medline
34. Bronevetsky, Y., Villarino, A. V., Eisley, C. J., Barbeau, R., Barczak, A. J., Heinz, G. A., Kremmer, E., Heissmeyer, V., McManus, M. T., Erle, D. J., Rao, A., and Ansel, K. M. (2013) T cell activation induces proteasomal degradation of Argonaute and rapid remodeling of the microRNA repertoire. *J. Exp. Med.* **210,** 417–432 CrossRef Medline
35. Johnston, M., Geoffroy, M. C., Sobala, A., Hay, R., and Hutvagner, G. (2010) HSP90 protein stabilizes unloaded argonaute complexes and microscopic P-bodies in human cells. *Mol. Biol. Cell* **21,** 1462–1469 CrossRef Medline
36. Adams, B. D., Claffey, K. P., and White, B. A. (2009) Argonaute-2 expression is regulated by epidermal growth factor receptor and mitogen-activated protein kinase signaling and correlates with a transformed phenotype in breast cancer cells. *Endocrinology* **150,** 14–23 CrossRef Medline
37. Rybak, A., Fuchs, H., Hadian, K., Smirnova, L., Wulczyn, E. A., Michel, G., Nitsch, R., Krappmann, D., and Wulczyn, F. G. (2009) The let-7 target gene mouse lin-41 is a stem cell specific E3 ubiquitin ligase for the miRNA pathway protein Ago2. *Nat. Cell Biol.* **11,** 1411–1420 CrossRef Medline

38. Hamilton, A. M., Oh, W. C., Vega-Ramirez, H., Stein, I. S., Hell, J. W., Patrick, G. N., and Zito, K. (2012) Activity-dependent growth of new dendritic spines is regulated by the proteasome. *Neuron* **74,** 1023–1030 CrossRef Medline
39. Bingol, B., Wang, C. F., Arnott, D., Cheng, D., Peng, J., and Sheng, M. (2010) Autophosphorylated CaMKIIα acts as a scaffold to recruit proteasomes to dendritic spines. *Cell* **140,** 567–578 CrossRef Medline
40. Bingol, B., and Sheng, M. (2011) Deconstruction for reconstruction: the role of proteolysis in neural plasticity and disease. *Neuron* **69,** 22–32 CrossRef Medline
41. Bingol, B., and Schuman, E. M. (2006) Activity-dependent dynamics and sequestration of proteasomes in dendritic spines. *Nature* **441,** 1144–1148 CrossRef Medline
42. Ehlers, M. D. (2003) Activity level controls postsynaptic composition and signaling via the ubiquitin-proteasome system. *Nat. Neurosci.* **6,** 231–242 CrossRef Medline
43. Smibert, P., Yang, J. S., Azzam, G., Liu, J. L., and Lai, E. C. (2013) Homeostatic control of Argonaute stability by microRNA availability. *Nat. Struct. Mol. Biol.* **20,** 789–795 CrossRef Medline
44. Leung, A. K. (2015) The whereabouts of microRNA actions: cytoplasm and beyond. *Trends Cell Biol.* **25,** 601–610 CrossRef Medline
45. Decker, C. J., and Parker, R. (2012) P-bodies and stress granules: possible roles in the control of translation and mRNA degradation. *Cold Spring Harb. Perspect. Biol.* **4,** a012286 Medline
46. Horman, S. R., Janas, M. M., Litterst, C., Wang, B., MacRae, I. J., Sever, M. J., Morrissey, D. V., Graves, P., Luo, B., Umesalma, S., Qi, H. H., Miraglia, L. J., Novina, C. D., and Orth, A. P. (2013) Akt-mediated phosphorylation of argonaute 2 downregulates cleavage and upregulates translational repression of MicroRNA targets. *Mol. Cell* **50,** 356–367 CrossRef Medline
47. Zeng, Y., Sankala, H., Zhang, X., and Graves, P. R. (2008) Phosphorylation of Argonaute 2 at serine-387 facilitates its localization to processing bodies. *Biochem. J.* **413,** 429–436 CrossRef Medline
48. Sahin, U., Lapaquette, P., Andrieux, A., Faure, G., and Dejean, A. (2014) Sumoylation of human argonaute 2 at lysine-402 regulates its stability. *PLoS ONE* **9,** e102957 CrossRef Medline
49. Takumi, Y., Ramírez-León, V., Laake, P., Rinvik, E., and Ottersen, O. P. (1999) Different modes of expression of AMPA and NMDA receptors in hippocampal synapses. *Nat. Neurosci.* **2,** 618–624 CrossRef Medline
50. Rao, A., and Craig, A. M. (1997) Activity regulates the synaptic localization of the NMDA receptor in hippocampal neurons. *Neuron* **19,** 801–812 CrossRef Medline
51. Nimchinsky, E. A., Sabatini, B. L., and Svoboda, K. (2002) Structure and function of dendritic spines. *Annu. Rev. Physiol.* **64,** 313–353 CrossRef Medline
52. Huganir, R. L., and Nicoll, R. A. (2013) AMPARs and synaptic plasticity: the last 25 years. *Neuron* **80,** 704–717 CrossRef Medline
53. Sala, C., and Segal, M. (2014) Dendritic spines: the locus of structural and functional plasticity. *Physiol. Rev.* **94,** 141–188 CrossRef Medline
54. Cougot, N., Bhattacharyya, S. N., Tapia-Arancibia, L., Bordonné, R., Filipowicz, W., Bertrand, E., and Rage, F. (2008) Dendrites of mammalian neurons contain specialized P-body-like structures that respond to neuronal activation. *J. Neurosci.* **28,** 13793–13804 CrossRef Medline
55. Zeitelhofer, M., Karra, D., Macchi, P., Tolino, M., Thomas, S., Schwarz, M., Kiebler, M., and Dahm, R. (2008) Dynamic interaction between P-bodies and transport ribonucleoprotein particles in dendrites of mature hippocampal neurons. *J. Neurosci.* **28,** 7555–7562 CrossRef Medline
56. Juvvuna, P. K., Khandelia, P., Lee, L. M., and Makeyev, E. V. (2012) Argonaute identity defines the length of mature mammalian microRNAs. *Nucleic Acids Res.* **40,** 6808–6820 CrossRef Medline
57. Patranabis, S., and Bhattacharyya, S. N. (2016) Phosphorylation of Ago2 and subsequent inactivation of let-7a RNP-specific MicroRNAs control differentiation of mammalian sympathetic neurons. *Mol. Cell. Biol.* **36,** 1260–1271 CrossRef Medline
58. Jarome, T. J., and Helmstetter, F. J. (2013) The ubiquitin-proteasome system as a critical regulator of synaptic plasticity and long-term memory formation. *Neurobiol. Learn. Mem.* **105,** 107–116 CrossRef Medline
59. Eacker, S. M., Dawson, T. M., and Dawson, V. L. (2013) The interplay of microRNA and neuronal activity in health and disease. *Front. Cell. Neurosci.* **7,** 136 Medline
60. Im, H. I., and Kenny, P. J. (2012) MicroRNAs in neuronal function and dysfunction. *Trends Neurosci.* **35,** 325–334 CrossRef Medline
61. Zeitelhofer, M., Macchi, P., and Dahm, R. (2008) Perplexing bodies: the putative roles of P-bodies in neurons. *RNA Biol.* **5,** 244–248 CrossRef Medline
62. Nalavadi, V. C., Muddashetty, R. S., Gross, C., and Bassell, G. J. (2012) Dephosphorylation-induced ubiquitination and degradation of FMRP in dendrites: a role in immediate early mGluR-stimulated translation. *J. Neurosci.* **32,** 2582–2587 CrossRef Medline
63. Kenny, P. J., Zhou, H., Kim, M., Skariah, G., Khetani, R. S., Drnevich, J., Arcila, M. L., Kosik, K. S., and Ceman, S. (2014) MOV10 and FMRP regulate AGO2 association with microRNA recognition elements. *Cell Rep.* **9,** 1729–1741 CrossRef Medline
64. Hauptmann, J., and Meister, G. (2013) Argonaute regulation: two roads to the same destination. *Dev. Cell* **25,** 553–554 CrossRef Medline
65. Shen, J., Xia, W., Khotskaya, Y. B., Huo, L., Nakanishi, K., Lim, S. O., Du, Y., Wang, Y., Chang, W. C., Chen, C. H., Hsu, J. L., Wu, Y., Lam, Y. C., James, B. P., Liu, X., *et al.* (2013) EGFR modulates microRNA maturation in response to hypoxia through phosphorylation of AGO2. *Nature* **497,** 383–387 CrossRef Medline
66. Yang, M., Haase, A. D., Huang, F. K., Coulis, G., Rivera, K. D., Dickinson, B. C., Chang, C. J., Pappin, D. J., Neubert, T. A., Hannon, G. J., Boivin, B., and Tonks, N. K. (2014) Dephosphorylation of tyrosine 393 in argonaute 2 by protein tyrosine phosphatase 1B regulates gene silencing in oncogenic RAS-induced senescence. *Mol. Cell* **55,** 782–790 CrossRef Medline
67. Swanger, S. A., and Bassell, G. J. (2011) Making and breaking synapses through local mRNA regulation. *Curr. Opin. Genet. Dev.* **21,** 414–421 CrossRef Medline
68. Schratt, G. M., Tuebing, F., Nigh, E. A., Kane, C. G., Sabatini, M. E., Kiebler, M., and Greenberg, M. E. (2006) A brain-specific microRNA regulates dendritic spine development. *Nature* **439,** 283–289 CrossRef Medline
69. Wayman, G. A., Davare, M., Ando, H., Fortin, D., Varlamova, O., Cheng, H. Y., Marks, D., Obrietan, K., Soderling, T. R., Goodman, R. H., and Impey, S. (2008) An activity-regulated microRNA controls dendritic plasticity by down-regulating p250GAP. *Proc. Natl. Acad. Sci. U.S.A.* **105,** 9093–9098 CrossRef Medline
70. Siegel, G., Obernosterer, G., Fiore, R., Oehmen, M., Bicker, S., Christensen, M., Khudayberdiev, S., Leuschner, P. F., Busch, C. J., Kane, C., Hübel, K., Dekker, F., Hedberg, C., Rengarajan, B., Drepper, C., *et al.* (2009) A functional screen implicates microRNA-138-dependent regulation of the depalmitoylation enzyme APT1 in dendritic spine morphogenesis. *Nat. Cell Biol.* **11,** 705–716 CrossRef Medline
71. Impey, S., Davare, M., Lesiek, A., Fortin, D., Ando, H., Varlamova, O., Obrietan, K., Soderling, T. R., Goodman, R. H., and Wayman, G. A. (2010) An activity-induced microRNA controls dendritic spine formation by regulating Rac1-PAK signaling. *Mol. Cell. Neurosci.* **43,** 146–156 CrossRef Medline
72. Taft, C. E., and Turrigiano, G. G. (2014) PSD-95 promotes the stabilization of young synaptic contacts. *Philos. Trans. R. Soc. Lond. B Biol. Sci.* **369,** 20130134 Medline
73. Ehrlich, I., Klein, M., Rumpel, S., and Malinow, R. (2007) PSD-95 is required for activity-driven synapse stabilization. *Proc. Natl. Acad. Sci. U.S.A.* **104,** 4176–4181 CrossRef Medline
74. Cane, M., Maco, B., Knott, G., and Holtmaat, A. (2014) The relationship between PSD-95 clustering and spine stability *in vivo*. *J. Neurosci.* **34,** 2075–2086 CrossRef Medline
75. Dong, C., Bach, S. V., Haynes, K. A., and Hegde, A. N. (2014) Proteasome modulates positive and negative translational regulators in long-term synaptic plasticity. *J. Neurosci.* **34,** 3171–3182 CrossRef Medline
76. Dong, C., Vashisht, A., and Hegde, A. N. (2014) Proteasome regulates the mediators of cytoplasmic polyadenylation signaling during late-phase long-term potentiation. *Neurosci. Lett.* **583,** 199–204 CrossRef Medline
77. Khoutorsky, A., Yanagiya, A., Gkogkas, C. G., Fabian, M. R., Prager-Khoutorsky, M., Cao, R., Gamache, K., Bouthiette, F., Parsyan, A., Sorge, R. E.,

Mogil, J. S., Nader, K., Lacaille, J. C., and Sonenberg, N. (2013) Control of synaptic plasticity and memory via suppression of poly(A)-binding protein. *Neuron* **78,** 298–311 CrossRef Medline

78. Hou, L., Antion, M. D., Hu, D., Spencer, C. M., Paylor, R., and Klann, E. (2006) Dynamic translational and proteasomal regulation of fragile X mental retardation protein controls mGluR-dependent long-term depression. *Neuron* **51,** 441–454 CrossRef Medline
79. Jarome, T. J., and Helmstetter, F. J. (2014) Protein degradation and protein synthesis in long-term memory formation. *Front. Mol. Neurosci.* **7,** 61 Medline
80. Leung, A. K., Calabrese, J. M., and Sharp, P. A. (2006) Quantitative analysis of Argonaute protein reveals microRNA-dependent localization to stress granules. *Proc. Natl. Acad. Sci. U.S.A.* **103,** 18125–18130 CrossRef Medline